Coherent integration of complex fringe visibility employing dispersion tracking

Jeffrey Meisner, Robert Tubbs, and Walter Jaffe

Leiden Observatory, P.O. Box 9513, 2300RA Leiden, The Netherlands

ABSTRACT

We discuss methods of interferometric data reduction using coherent integration of fringe visibility. Unlike incoherent estimation techniques which discard the phase of interference, coherent integration retains as a complex quantity the contribution from each frame (or scan). In order to integrate these coherently, one must apply an OPD correction (or "phase reference") to compensate for random atmospheric pathlength fluctuations.

In an instrument with substantial bandwidth, it is also necessary to correct for fixed and random dispersion. The integrity of phase functions obtained is dependent on correct modelling of fixed optical phase functions (obtained from a calibrator observation), dispersion from air filled delay-lines (calibratable in principle), and averaging over time to reduce the effect of random atmospheric water vapor dispersion.

To achieve the best performance, it is necessary to include a dispersion tracker as well as tracking achromatic OPD, applying each as a phase correction as a function of time and of optical frequency. Using MIDI, the N band instrument of the VLTI, which has a wide bandwidth, it is often possible to uninterruptedly track random dispersion fluctuations over an observation. Plots of dispersion fluctuations due to water vapor above the VLTI are shown, which are used (along with OPD tracking) to coherently integrate raw frames from that instrument.

The resulting complex visibility includes a unique phase delay signature reflecting the source structure. A residual "water-vapor-like" phase may be present due to unmonitored humidity in the delay line paths, and to incomplete averaging of (nominally zero-mean) atmospheric water vapor fluctuations. Nevertheless, the use of visibility phase results corrupted by random dispersion is possible.

Keywords: Stellar interferometry, differential phase, coherent integration, dispersion, water vapor, VLTI, MIDI, VINCI

1. INTRODUCTION

All interferometry is based on optical coherence. However among various instruments, configurations, and techniques, some propagate that coherence further and more precisely than others. Coherence in a system refers to the property of being directly sensitive to the phase of a signal propagating through that system. If and when a signal's phase is destroyed, for instance by taking the squared magnitude of a phasor, the system becomes incoherent at that point. There are various reasons that one would want to maintain coherence or go incoherent at various points in a system (or algorithm) depending on the technique in use.

1.1. Coherent Integration

The range of techniques and configurations covered by the term "Coherent Integration" is rather varied and will not be explored in detail here. The most essential aspect of coherent integration is summed up in Fig. 1 in which reference to a particular hardware configuration is intentionally left vague.

What is essential to the concept of coherent integration, is that a phase (or delay) determination is obtained from one interferometric observation, the so-called *reference channel* or *tracking channel*. A second interferometric observation (generally at a lower signal-to-noise ratio) is simultaneously obtained and has its phase de-rotated (or, equivalently, its delay shifted) using the reference phase determination. In a ground-based optical/IR interferometer, this addresses the essential need of correcting for atmospheric OPD fluctuations.

email: meisner@strw.leidenuniv.nl

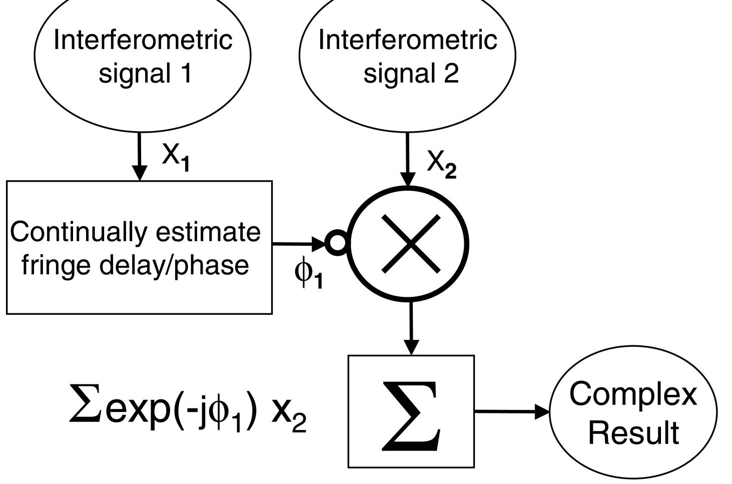

Figure 1. Essence of coherent integration. Fringe tracker provides continual estimate of atmospheric phase (possibly including dispersion). Phase of reference channel (1) is applied negatively to signal in channel 2. Cophased quantity is integrated over time, as noise averages toward zero.
Depending on configuration, correction of phase of channel 2 may occur in *hardware* in realtime, or may be applied *post-detection* using an offline estimate of $\phi_1(t)$ obtained from recorded data (see text).

The "correction" of the second channel using a phase reference from the tracking channel, may be effected in one of two ways. In a *hardware* based coherent integration system, correction of the second channel results from an active optical element (i.e. delay actuator) which, using the atmospheric OPD reference from the first channel, "freezes" the fringe so that it can be integrated as if the atmosphere were not present. Alternatively, it may be possible to obtain similar results *post-detection*, that is, in the data processing stage. In that configuration, the complex correlation measured at each point in time is multiplied by a phase factor $e^{-j\phi_1}$ where ϕ_1 is the phase measured by the tracking channel. In principle, the result from the two methods is identical. A combination of hardware and post-detection correction may also be employed.

1.2. Characteristics of Coherent Integration

An important point regarding the coherently integrated result, is that all phase effects which are common-mode between the two channels are cancelled out through the procedure, while phase effects which, for one reason or another, affect only one channel, are preserved in the phase of the result. The main emphasis of the remainder of this paper concerns the preservation, corruption, and calibration of such phase information when coherent integration of interfered light over a wide wavelength range is performed.

In addition to preserving phase information, subject to the above stipulation, coherent integration is able to achieve a better integrated signal-to-noise ratio than incoherent integration for weaker observations (when the SNR obtained during a period of τ_0 is not much larger than unity). Given a phase correction $e^{-j\phi_1(t)}$, coherently integrated visibility V is a *linear* estimate of the data in the measurement channel, and thus measurement noise averages toward (complex) zero. This is in contrast to incoherent integration, in which case it is $|V|^2$ that is integrated, and noise n contributes a D.C. term to the integrated visibility in the amount of $\langle n^2 \rangle$. This offset must be subtracted from the integrated result in order to obtain an unbiased estimate of the squared visibility, making the incoherent estimator dependent on proper estimation of the noise floor, which can be problematic,[1] particularly for weak observations.

Coherent addition of complex phasors means that the result directly depends on the phase integrity of the terms contributing to that sum. In addition to being an advantage of coherent integration, this also makes such techniques sensitive to any unmonitored or unmodelled differential phase effects between the science and reference channel. In particular, assume there is an unmonitored phase error ϕ affecting each frame, and that ϕ is gaussian with a mean $\bar{\phi}$ and standard deviation σ_ϕ. Then a coherent estimator will acquire a phase error of $\bar{\phi}$, and its amplitude will be reduced by the factor $exp(-\sigma_\phi^2/2)$.

Even if the result of coherent integration is properly understood and calibrated at one wavelength, there will be additional degradations in a *wideband* instrument both due to random atmospheric dispersion fluctuations, and to passage of the beams through unbalanced air filled delay-lines. This is a primary topic of this paper and will be discussed in detail below.

1.3. Applications of Coherent Integration

Here are some of the better known examples of coherent integration in optical interferometry; this is not intended as an exhaustive list but serves only to illustrate the scope of the concept and the relevance of the subsequent discussion.

- Coherently integrating a weak science signal at one wavelength using a phase reference at a second wavelength where the SNR is higher.[2]
- Similarly, in a spectrally-dispersed instrument, using a combined phase reference from a large number of spectral channels in order to coherently integrate each individual spectral channel.
- Coherently integrating weak spatially filtered signals in narrow spectral channels using a reference from a tracking channel which is wideband and/or less spatially filtered in order to maximize its SNR.[3]
- Coherently integrating a weak science signal along a long baseline (typically for which a star is over-resolved, having a small residual visibility) using a phase reference calculated from fringe tracking each of two (or more) shorter baselines which comprise the long baseline.[4]
- In a delay-scanning instrument, using an OPD estimate from the entire scanned fringe in order to coherently integrate each individual point along the fringe.[5]
- In a *dual feed* interferometer, using light from an off-axis reference star in order to coherently integrate the signal from a science object in order to obtain visibilities *including absolute phase* relative to the position of the reference object, which may be used for interferometric image reconstruction.
- In a dual feed interferometer, using light from a brighter star in one channel in order to coherently integrate the signal from a dimmer object in the other channel in order to measure the OPD difference between the two signals which supplies a precise *astrometric* determination of the separation between the stars.
- In a *nulling* instrument, using some light from the star (possibly at a different wavelength) in order to track the atmospheric OPD (and dispersion!) and rapidly adjust a hardware delay-line (and dispersion corrector) in order to maintain phase cancellation of starlight in the nulling channel.

In the case of the above applications, an additional distinction could be mentioned between systems using realtime *hardware* correction of the optical delay in order to effect coherent integration, and configurations in which the correction is applied post-detection. However one must use hardware correction in the case that one intends to employ a long exposure on a detector in order to combat the effect of detector noise. Obviously correction in hardware is also mandatory for the case of *nulling* interferometry. In the remaining cases, off-line (post-processing) cophasing of the detected signal is generally simpler, and has the additional advantage that the reference phase applicable to a given time, may be computed using future, as well as past data from the reference interferometer.

For the remainder of this paper, we shall consider coherent integration of data obtained from a single interferometer, observing a single target, in which the phase reference is obtained from the entirety of the data, and then applied to the data individually. Specific results are thus obtained from the MIDI (N band) and VINCI (K band) instruments of the VLTI. In the case of MIDI, detection is performed using spectral dispersion from which an estimate of the atmospheric OPD and dispersion can be obtained and applied to each optical frequency component individually. In the case of VINCI, the fringe is scanned in delay, again from which an estimate of the atmospheric OPD is possible, enabling coherent integration of the entire fringe.[5]

Although we will concentrate on such examples, most of the discussion is more or less applicable to each of the techniques listed above. For instance, use of an off-axis star in a wideband system faces exactly the same concerns (plus the issue of anisoplanicity). And baseline bootstrapping also faces the same concerns except that there are now two (or more) fringe trackers to consider.

2. DISPERSION AND WIDEBAND OPTICAL SYSTEMS

We will briefly cover the mathematical basis of phase functions and dispersion. Most familiar optical components, including everything inbetween the star and an interferometer's photodetector, fall in the class of *linear systems.* Thus, in the frequency domain, transmission of a single spatial (and single polarization) mode through any such optical train, is fully described by a single complex value at every frequency. If x_1 is the input and x_2 is the output, then:

$$x_2(\nu) = H(\nu)x_1(\nu) = |H(\nu)|e^{j\phi(\nu)}x_1(\nu) \quad .$$

In the present context we are not interested in the amplitude transmission $|H(\nu)|$, only in the phase response. It is the phase response, $\phi(\nu)$ that describes all delays and dispersion.

2.1. Delay, Phase, and Dispersion

To illustrate the following concepts, let us consider propagation of light in the K band (120 - 150 THz) through one meter of air, for which we have plotted the phase as a function of frequency, $\phi(\nu)$, in Fig. 2A. We plot the phase only over the frequency limits we are considering, 120 - 150 THz, but include a dashed line which is an extrapolation of the (approximately) linear function over this range, that appears to intersect the origin.

2.1.1. Removal of achromatic delay

In Fig. 2A, we see a huge phase function $\phi_1(\nu)$, dominated by achromatic delay. An achromatic delay τ has a phase proportional to optical frequency:

$$\phi(\nu) = 2\pi\nu\tau \quad .$$

Even if there were no air present, there would be a phase delay through passage of 1 meter of vacuum given by $2\pi\nu\tau_0$, where τ_0 is approximately 3.335 nanoseconds. If we subtract this achromatic phase from $\phi_1(\nu)$, then we are left with the phase shift $\phi_2(\nu)$ due only to the air present, shown in Fig. 2B. This, then, is the phase function that an interferometer would observe, for instance, if an air filled delay-line of exactly 1 meter were used to compensate for exactly 1 meter of geometrical path excess in space.

This is still a huge phase, mainly reflecting the non-dispersive component of the index of refraction of air. For instance, at 135 THz (2.22 μm) the normalized refractivity of air, $\hat{n}_{air}$ is approximately 21.51 fs/$(mole/m^2)$. A meter of air at STP contains 44.6 $mole/m^3$. Thus at that wavelength a phase delay of τ_1 = 959 fs is experienced due to the air. Let us subtract the phase due to that delay given by $2\pi\nu\tau_1$. Again, we could view this as the result that would be obtained if a 1 meter air filled delay line were used to compensate for a geometric path length of 1.000287 meters in space. We are now left with a phase function, plotted in Fig. 2C.

2.1.2. First order dispersion

After zeroing the phase delay, the *slope* of the phase function in Fig. 2C is due to *first order dispersion.* It is described uniquely by the *group phase* Φ_G which can be read off of the graph as the y-intercept of the extrapolation of this (approximately) linear function over the optical frequency range of concern. In this case we see a slope which sets Φ_G = -1.9 radians. Note that it is *not* the slope per se which determines the group phase, except in the special case that the phase delay has been adjusted to zero. This is illustrated in Fig. 2D where various small achromatic delays have been added to the phase function, thus changing its slope. All of these functions have the same dispersion, as can be seen by their extrapolations. Even the huge phase functions of Fig. 2A and B (before we subtracted the vacuum delay and the average additional air delay, respectively), if viewed in sufficient detail, would be seen to also intercept the y axis at exactly -1.9 radians!

2.1.3. Group delay

All of the phase functions shown in Fig. 2D after adding various amounts of achromatic delay, contain the same dispersion. In addition to the one at which the phase delay at midband has been adjusted to zero phase, another one stands out. Plotted in bold, is the phase function in which the *group delay* has been cancelled with an achromatic delay $-\tau_g$. The group delay can be thought of as the unique delay point at which all optical frequencies (within the range of concern) find themselves in approximately the same phase (not necessarily zero

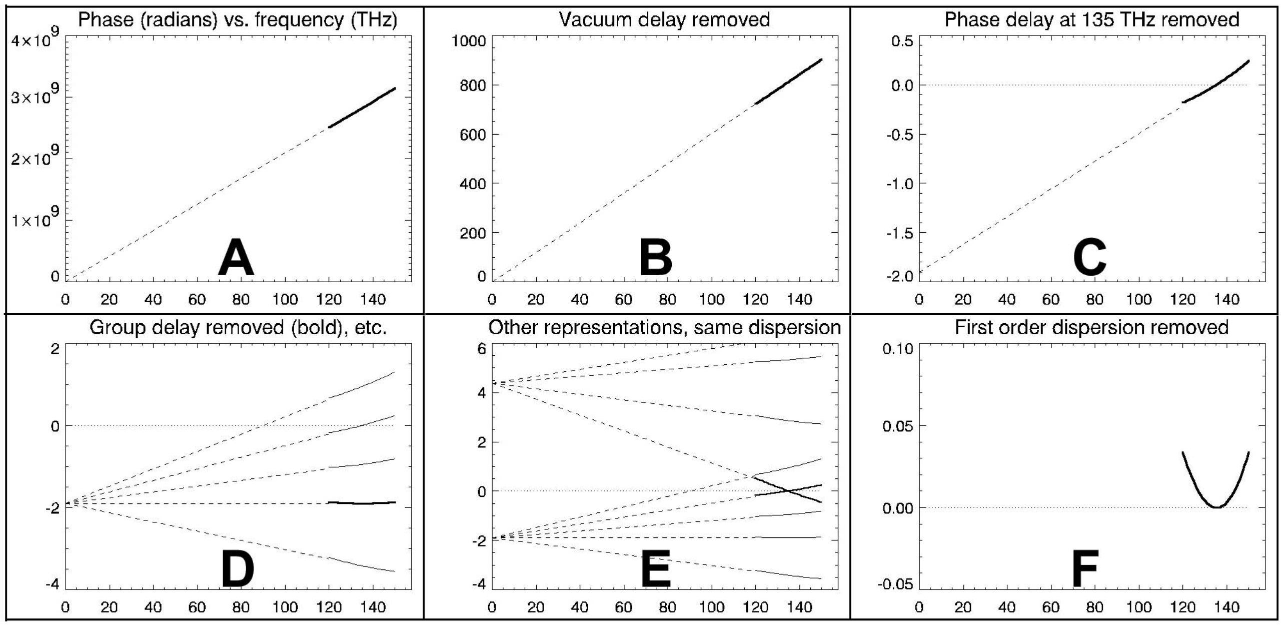

Figure 2. A-E: Transmission through 1 meter of dry air at STP, shown with various levels of achromatic OPD removed. Y intercept of the dashed lines extrapolated from these phase functions, always indicates the group phase due to first order dispersion of that amount of air. **F:** Removal of first order phase function, reveals higher order dispersion.

phase); thus this curve is horizontal. That phase that applies equally to all frequencies at the group delay point, is, again, the group phase Φ_G.

Clearly if the first order dispersion had been of a different amount, then adjusting the achromatic delay to again cancel the group delay would again lead to a horizontal plot, but with a different offset in y, i.e. a different group phase. For this reason, first order dispersion is sometimes referred to as a "constant phase" function; we can see from the various plots in Fig. 2D that "constant phase" is but one possible description. It is also often referred to as an "achromatic phase shift," which, although understandable, is rather a misnomer, inasmuch as a constant phase over frequency, other than $2\pi N$, is *very* chromatic!

2.1.4. Mathematical description

For reference, we mention the standard definitions of phase delay $\tau(\nu)$ and group delay $\tau_g(\nu)$, in terms of the phase function $\phi(\nu)$, as can be found in any elementary physics text:

$$\tau(\nu) = \frac{\phi(\nu)}{2\pi\nu} \quad , \quad \tau_g(\nu) = \frac{1}{2\pi}\frac{d\phi(\nu)}{d\nu} \quad . \tag{1}$$

Then the group phase can be expressed mathematically, as the offset between the phase and group delays, converted to a phase angle:

$$\Phi_G(\nu) = 2\pi\nu(\tau(\nu) - \tau_g(\nu)) \quad . \tag{2}$$

2.1.5. Description in terms of known phase delay

In order for the expression for the phase delay in (1) to return the expected result, the $\phi(\nu)$ used must be a properly unwrapped phase; otherwise an ambiguity remains amounting to an integer number of wavelengths, N/ν. This must also be correctly inserted into (2) in order for the calculated group phase to be returned as an unwrapped phase; otherwise its validity is only modulo 2π. These ambiguities are avoided if one starts with *phase delay* $\phi(\nu)$ as the basis for all calculations. From that we can calculate:

$$\Phi_G(\nu) = -2\pi\nu^2\frac{d\tau(\nu)}{d\nu} \quad , \tag{3}$$

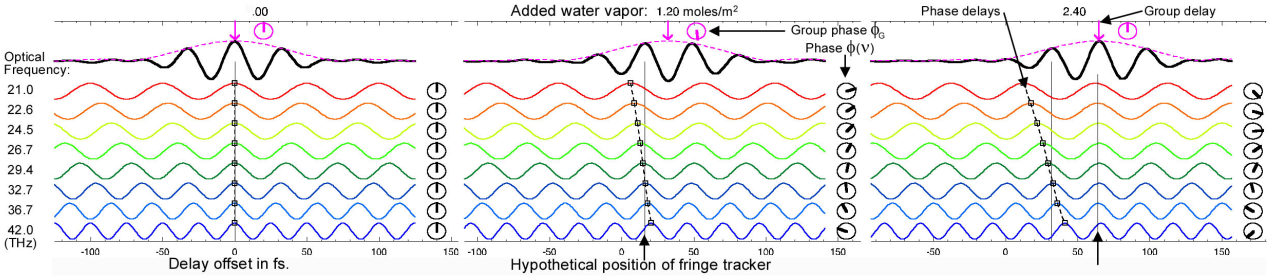

Figure 3. Decomposition of the combined fringe (top) into 8 optical frequency components over the N band. **Left:** Assume we are tracking on the central fringe with zero dispersion. All frequency components are at zero phase at the tracking OPD. **Center:** With 1.2 $mole/m^2$ of differential water vapor, the group phase has increased to approximately π radians. Most frequency components now have a significant phase shift relative to the tracking point. The peak value of the combined fringe (top) on which we are tracking, has been reduced and is no longer higher than the adjacent fringe peak. **Right:** With 2.4 $mole/m^2$ of differential water vapor, there has been a complete 2π rotation of the group phase, and, viewed from the position of the bottom arrow, resembles the diagram on the left with no dispersion (except for a small amount of high order dispersion). However at the tracking point most frequency components have a large phase shift. If the fringe tracker had noticed the problem and made a sudden jump to the new peak fringe, then the phases in the coherently integrated result would depend on exactly when that jump occurred, leading to a a chaotic result.

$$\tau_g(\nu) = \tau(\nu) - \frac{\Phi_G(\nu)}{2\pi\nu} = \tau(\nu) + \nu\frac{d\tau(\nu)}{d\nu} \quad . \tag{4}$$

This approach is useful whenever one is considering phase shifts resulting from propagation of light through a material with a specified refractive index $n(\nu)$. In the case of sparse gasses, we use the normalized refractivity[6] $\hat{n}(\nu)$ from which one can express the ordinary refractive index as $n(\nu) = 1 + \rho c\,\hat{n}(\nu)$ where ρ is the density of the gas in $mole/m^3$. In general, propagation through a column density ρL of a sparse gas introduces a phase delay:

$$\tau(\nu) = \hat{n}(\nu)\rho L + \tau_0 \quad . \tag{5}$$

where the second term, τ_0, is the vacuum delay that would be experienced without any gas present: $\tau_0 = L/c$.

2.1.6. The dispersion constant K

Using the dispersive delay as expressed in (5) we can then calculate the magnitude of first order dispersion using (3):

$$\Phi_G(\nu) = -2\pi\nu^2\frac{d\tau(\nu)}{d\nu} \quad = -2\pi\nu^2\frac{d\hat{n}(\nu)}{d\nu} = -K(\nu)\rho L \quad , \tag{6}$$

where **K** is the *dispersion constant*:

$$K(\nu) = 2\pi\nu^2\frac{d\hat{n}(\nu)}{d\nu} \quad . \tag{7}$$

Thus **K** is the sensitivity of group phase to column density of a particular gas (or gas mixture). The result of a calculation using (6) is clearly an *unwrapped* group phase. Note that when only first order dispersion is present then **K** is constant over the applicable range of frequencies.

2.1.7. Higher order dispersion

We have seen that dispersion due to a quantity of a sparse gas can be quantified in terms of its unwrapped group phase, and can easily be observed in terms of that group phase modulo 2π. However if one looks closely at the phase function shown in Fig. 2C-E, a small deviation can be seen from the straight dashed line which intercepts the y axis at Φ_G. This is thus *higher order* dispersion, which is not accounted for by Φ_G. If we were to remove the first order dispersion component from the dispersion function in Fig. 2A-E, we would obtain the smaller (but not insignificant) higher order dispersion predicted for 1 meter of dry air in the K band. This is plotted in Fig. 2F.

Higher order dispersion is very much unlike first order dispersion, inasmuch as it does not wrap around 2π but is steadily cumulative. Thus with passage through about 100 meters of such air, instead of only 1 meter, the group phase would have wrapped around 2π 30 times, but the magnitude of the higher order component in Fig. 2F would be multiplied by 100. Such visibility phases in the K band have been directly observed using VINCI (Fig. 6B), albeit with some quantitative disagreement (see Sect. 4.2).

2.2. Interpreting Wrapped Phase Functions

We can easily produce *wrapped* phase functions, from any given phase delay function (such as would be predicted from material dispersion). However the inverse procedure can not generally be performed unambiguously. This applies in two important cases.

In the case of "lumped dispersion" we might be able to describe the transfer function of a "black box" in terms of phase, but cannot translate this to phase delay. For instance, if two polarizations passing through a half-wave plate, have a relative phase shift of π, one cannot say that one or the other polarization is "delayed" by $1/2\nu$ relative to the other. One could just as well claim that one beam suffers a $7/2\nu$ phase delay, and that would be perfectly consistent with any experiment that could be imagined.

Such an inability to identify an unambiguous phase delay also applies to phase measurements obtained by an interferometer: we only directly measure a phase *angle*, not the delay directly.

From the wrapped phase, one can always calculate the group delay using (1), which may be sufficient. If one also has an estimate of (or a tight upper limit on) dispersion present in the interference, then the correct branch of the phase function can be inferred. But without such extra information, only a wrapped phase is measured, to which $2\pi N$ can be arbitrarily added.

Because an interferometric signal (without phase referencing on a second star) also has an unknown zero-point delay, this means that there are *two* free parameters accompanying such a measured phase function: the unknown zero-delay point, and an integer number of 2π phase rotations. This is illustrated in Fig. 2E, in which a number of different phase functions are plotted which are consistent with the visibility phase that might have been measured by an interferometer.

However it is nevertheless possible to compare measured phase functions with each other or with a model, despite these free parameters. This is best done by first transforming the phases to *phase delays* using (1) and adjusting the offset of one delay in order to make the average delays of the two match. Then one may either compare the two phase delay functions, or the two phase functions (after delay adjustment) themselves. The only difference is an additional weighting present (according to ν^1) when comparing the phases themselves, since $\phi = 2\pi\nu\tau$ (in any case, for optimum sensitivity one needs to form a custom weighting function based on the SNR obtained over the frequency band).

There will still be a number of discrete branches possible by adding $2\pi N$ to the phase before forming the phase delay. However in a normal case, these can be resolved by inspection: most of the possibilities will have a large slope of phase delay at the center frequency. Often one, and at most two, will have a clearly minimum slope at a specified center frequency, thus at most two comparisons need to be made. However if this is not kept in mind, one could carelessly create a clever computer program that fails to notice, for instance, any similarity between the two bold plots of Fig. 2E!

2.3. Refractive Indices of Atmospheric Gasses

Water vapor is responsible for most of the *random* dispersion affecting interferometry in the infrared, however the dispersion of dry air is important as well due to large columns of air in delay-lines which are unbalanced between the arms of an interferometer. We have utilized a recently published calculation[7] for the refractivity of water vapor in the infrared (a similar but independent calculation[8] arrives at the same dispersion). The normalized refractivity $\hat{n}$ of water vapor as a function of wavelength in the infrared is shown in Fig. 4.

Both papers have also calculated the refractivity of CO_2 in the infrared. We employ the classical formulae[9] for the refractivity of dry air in the visible due to ultraviolet transitions, but we add the refractive contribution due to CO_2 in the amount of 370 parts per million. This produces a model that we expect to be valid at all infrared

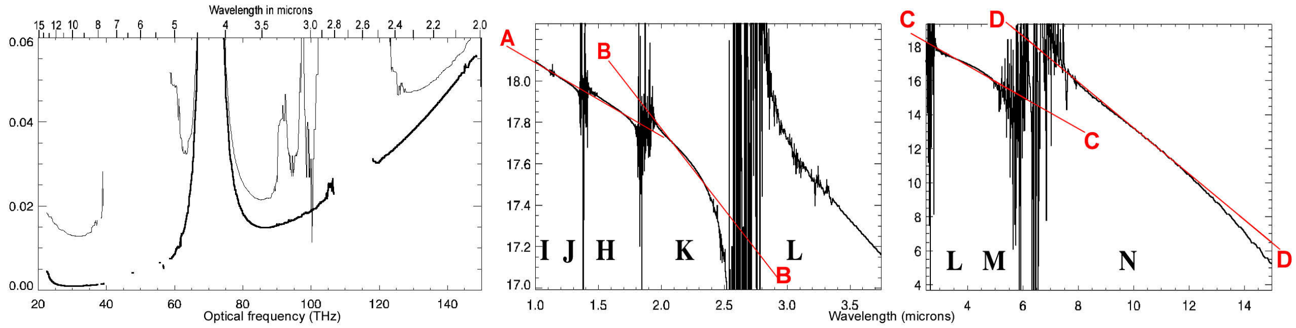

Figure 4. Left: Dispersion constant **K** of dry air (lower bold curve) and for air with .5% water vapor content (thin plot), as might be experienced in the air filling a long delay-line. **Right:** Normalized refractive index $\hat{n}$ of water vapor versus wavelength in microns, in two ranges. Slopes in regions over which dispersion is largely first order (quasi-constant dispersion constant **K**) are indicated with lines labelled A (I, J, and H bands, $\mathbf{K} \approx .7$), B (K band, $\mathbf{K} \approx 1.5$), C (L and M bands, $\mathbf{K} \approx 1.8$), and D (N band, $\mathbf{K} \approx 2.5$).

wavelengths, including particularly the 3.5 micron (L) and 5 micron (M) bands which are strongly affected by CO_2 dispersion.

However it is nevertheless proposed that actual measurements of refractivity be undertaken rather than just relying on computations. That would allow for use of the approach that is proposed for correction of the effect of these dispersive substances with confidence at the milli-radian level.

3. WIDEBAND COHERENT INTEGRATION AND DISPERSION

Coherent integration of a narrowband signal using a narrowband reference at the same optical frequency, is relatively straightforward. A measurement of the phase of the reference is negated and applied to the fainter signal in the other channel. Identification of the "central" fringe in this case is not an issue: any phase peak supplies an equally good phase estimate to cophase the other channel.

In the wideband case, things become more complicated. We need to obtain a phase reference to cophase the second interferometric channel. If there is random dispersion present, then two complications are introduced. *Tracking* the atmospheric OPD becomes problematic,[10] as is suggested in Fig. 3, which depicts increasing water vapor dispersion in a realistic amount. Secondly *correction* of the phase of each spectral component, (again as depicted in Fig. 3) is no longer possible using a single determination of atmospheric OPD.

What solutions may exist to allow coherent integration in the face of such problems? Here are a few approaches and their characteristics:

- *Reduced total bandwidth.* Although this largely resolves the problems, it also defeats the advantages of coherent integration. This reduces the sensitivity of the method, and greatly limits the breadth of information obtained from the interferometric observation.

- *Shorter coherent periods.* This has enabled successful coherent integration in the visible where decoherencing due to "differential refraction" and fringe jumping are dominant problems. However it also means that the results are forced into incoherent estimation, entailing loss of phase information that might otherwise be available.

- *Quasi-coherent integration.* This is a very practical and robust method. Instead of tracking directly on a fringe *phase* peak, a slower (but thereby more robust) tracking algorithm follows the group delay peak, while ignoring the precise position of the phase peak. Thus the effect of the scenario of Fig. 3, where the original phase peak gradually becomes a secondary peak, is not problematic, inasmuch as the shifting of the group delay peak is always smooth and trackable.

However the precision of a group delay estimate is much poorer than a phase estimate, and thus generally inadequate for cophasing. Moreover, with non-zero dispersion, the phase of each frequency component at the group delay point departs from zero. But because they vary together, in each frame the average phase over all spectral channels at the position of the group peak is found (i.e. the group phase), and used, along with the group delay estimator, to synthesize a phase reference for cophasing each spectral channel. This procedure is valid over wavelength ranges where the form of random dispersion (due to atmospheric water vapor) is approximately first order, as is indicated by lines **A** - **D** in Fig. 4.

This approach has been very successful in reducing delay scanned data from VINCI[5] and more recently, spectrally dispersed data from MIDI.[1] One drawback is that, by tracking on the group delay, it is totally insensitive to first order phase (but, fortunately, that includes first order dispersion!) in the source spectrum. Another drawback, is that while it does retain higher order phase information from the source, it also folds into its estimate any residual high order dispersion, since it has not tracked the dispersion in detail.

- *Coherent integration with dispersion tracking.* In this case, two separate tracking estimators run through the data in parallel. One tracks achromatic OPD variations, the other follows fluctuations in the group phase caused by water vapor dispersion fluctuations. The result of each estimator is applied to cancel the effect of OPD and water vapor dispersion respectively, so that the partially corrected signal can be better employed by the other estimator.

  This approach is currently in development for use with MIDI data and was used for the reduction of the 8 MIDI observations plotted in Fig. 5C (see Sect. 4.3). The detailed results of one such reduction are shown in the graphs of Fig. 7. The atmospheric OPD and water vapor processes are included as intermediate results. These have been modelled along with the average phase function, which is returned as part of the result. Together these three results produce a phase reference from which the data is coherently integrated, thereby refining the estimates of these intermediate products, as well as the correlated amplitude which is also shown in Fig. 7.

  However this coherent procedure is much more drastically affected by signal dropouts or other unanticipated effects which disturb the continuous tracking of the OPD and water vapor estimates. Its development remains a topic of ongoing research.

3.1. Corruption of Visibility Phase by Dispersion

Following are potential sources of non-zero phase which we can identify.

3.1.1. Zero-mean dispersion effects

The following dispersive effects are expected to have a zero (long-term) mean, and therefore will have, at most, a second-order effect on coherent integration (if they are not tracked out) in the case that their rms amplitudes are not much smaller than a radian.

- *Random Atmospheric Water Vapor.* Atmospheric water vapor inhomogeneities are a major source of random longitudinal dispersion affecting interferometry at all infrared wavelengths.[6,8] Although the differential path should have a zero mean value of water vapor column density, incomplete averaging over the duration of an observation may leave a significant residual (discussed below). And of course this is a large source of dispersion which *must* be tracked and corrected in real-time in order for wideband *nulling*[11] to be successful.

- *Differential Refraction.* This is a major concern at visible wavelengths.[12] However its magnitude at infrared wavelengths is reduced to insignificance, and will not be further considered in the present context.

3.1.2. Dispersion offsets

The following effects introduce phase functions which *are* expected to be present in the results of coherent integration:

- *Optical Train.* There will naturally be dispersive phase functions attributable to optical components. Although, in most interferometers, the beam paths are designed symmetrically, there will be a residual phase from the beam combiner in particular, and from any inadvertent imbalances in the optical system. Fortunately this component of the phase function is constant, and can thus be extracted from a calibrator observation and used to obtain a calibrated phase function (with the free parameters, discussed above).
- *Unbalanced Delay-Line Air Paths.* The dispersion due to (humid) air in delay-lines and other light paths is a large source of dispersion, which, in principle, can be monitored and compensated for. This is examined in more detail below (Sect. 3.2.1).
- *Residual Non-Averaged Component of Random Atmospheric Dispersion.* Because random differential atmospheric water vapor column densities include large low temporal frequency components,[13] we expect that substantial residual amounts of water vapor dispersion will remain in the coherently averaged spectra from observations of reasonable duration. In Sect. 4.1 we believe we have measured (or, at least, set an upper limit on) the magnitude of such residual dispersion affecting short observations (2 - 3 minutes) at the VLTI, albeit over a short baseline.
- *Source Phase.* Of course this is what we wanted to measure in the first place! It gets added to the three previous offsets to produce a result which can thus be interpreted to the extent that these can effects can be calibrated.

3.2. Estimation of Visibility Phase

Finally, one can attempt to obtain a useful visibility phase function (subject to the free parameters discussed in Sect. 2.2). This requires cancellation of the delay-line air dispersion, as well as it can be known, and cancellation of the instrumental phase function. The latter is obtained from a calibrator observation, that is, from observing a star that is unresolved, or, at least, known to be symmetric (thus zero phase). Finally it may be possible to infer the non-averaged component of atmospheric water vapor dispersion, within certain constraints of a model.

3.2.1. Calibration of dispersion due to differential delay-line air paths

A large component of dispersion affecting interferometric observations is attributable to the passage through air filled light paths *inside* the interferometer infrastructure, including the delay-lines. It is possible that a term of this sort will occur due to asymmetries in the interferometer or passage of the two beams through air of different temperatures or humidities; a study is underway to quantify such non-uniformities inside the VLTI.[14]

However even assuming symmetry in all aspects of the interferometer, a residual dispersion will result when air filled delay-lines are employed. Let L denote the differential delay-line travel employed to compensate for the geometric delay resulting from the position of the target on the sky in relation to the interferometer's baseline. In addition to the vacuum delay over this length of L/c, there will be an additional (and dispersive) phase delay at optical frequency ν given by

$$\Delta\tau(\nu) = \hat{n}(\nu)\rho L \quad , \tag{8}$$

where ρ is the density of the air in $mole/m^3$ and $\hat{n}$ is the refractivity of the air (taking into account its humidity and composition in detail) in fs/$(mole/m^2)$. Thus this is a dispersive component which can, in principle, be modelled with accurate knowledge of ρ (dependent on the temperature and barometric pressure) and $\hat{n}$ (dependent on the humidity). Correction for (8) is then performed on the phase $\phi(\nu)$ measured through coherent integration as follows:

$$\phi_{corr}(\nu) = \phi_{raw}(\nu) - 2\pi\nu\rho L\hat{n}(\nu) \quad . \tag{9}$$

3.2.2. Estimating large group phases in the source spectrum

In a small number of interesting cases, the group phase of the resulting phase estimation will itself be of interest. This will never be measurable with a great accuracy due to the additive effect of an unknown average water vapor column density (see Sect. 3.1.2). However a gross group phase in the visibility result may still be observable.[15]

One such example is shown in Fig. 5B where the raw group phase of an observation of α ori stands out. Its measured group phase relative to the fit for delay-line air (thus calibrating for its dispersion as discussed above) is highly inconsistent with 0^o. In fact in this particular case, α ori had been observed beyond the first visibility null, so that a group phase of π would have been expected. Surprisingly, however, the measured group phase found was 137^o which is *marginally* inconsistent with 180^o, inasmuch as the rms scatter due to incomplete averaging of water vapor observed was about 18^o (see Sect. 4.1). If significant, this could be an indication of source asymmetry. A longer observation may have been able to better ascertain the significance of this 43^o discrepancy in the group phase.

However even much longer observations will never be able to lower the effect of residual water vapor dispersion to values a great deal smaller than the .25 $mole/m^2$ rms level of scatter obtained in the observations plotted in Fig. 5B. Thus direct measurement of the visibility group phase (without employing more powerful observational techniques) will never be possible with any degree of precision.

3.2.3. Correction of residual water vapor dispersion in coherently integrated results

Depending on *a priori* constraints regarding the source phase function we are measuring, it should sometimes be possible to obtain an *exact* determination of the water vapor column whose dispersion is affecting a coherently integrated result. This is possible as a function of the group phase of the underlying visibility function, which thus becomes a free parameter in the result. This may be useful, for instance, when we are expecting only a small deviation from a zero phase function, and can thus insist that the underlying group phase is zero (or in general, a function of a parameter that is being fit to the model).

We do this by assuming that some amount of additional water vapor is present in the phase of the result (after correction for delay-line air), and note that the measured group phase must be equal to the (known) group phase of the model plus the group phase of an unknown water vapor column density w:

$$\Phi_G\ (measured)\ =\ \Phi_G\ (model) + Kw \quad , \tag{10}$$

where **K** is the dispersion constant for water vapor at the wavelength band in use. There is only one complication in determining w using (10). That is because the measured group phase is a wrapped phase, and can only be measured modulo 2π.

We can see, in Fig. 3, that as water vapor is added to the path, the group phase increases, but winds around to 0 after the addition of about 2.40 $mole/m^2$. Let us call that quantity $w_0 = 2\pi/K$ a "bucket" of water vapor. Adding an integer number of buckets of water vapor has no effect on the group phase, but contributes a non-negligible high order phase function. For instance, in the K band $w_0 = 4.42\ mole/m^2$, and one bucket has a higher order phase function (over 125 - 150 THz) of rms magnitude 2.5^o.

Since $Kw_0 = 2\pi$, (10) can be satisfied (for wrapped phases) with the addition of any integer number of buckets of unmonitored water vapor dispersion. However accidently adding an extra bucket of water vapor will introduce the *higher order* dispersion phase from that much water vapor into a calibrated phase determination! In order to avoid such a possibility, it is necessary to be able to model *a priori* the water vapor column with confidence to better than $w_0/2$. Then one is assured that the *unwrapped* value of w in (10) is less than $w_0/2$, and can thus be solved for unambiguously by simply choosing the closest branch.

In principle this method should allow measurement of tiny phase signatures even in the presence of much larger water vapor dispersion which is not directly monitored. However the only component of the resulting phase function which is meaningful, is that part which is *not* degenerate with the refractivity of water vapor, as this has been allowed as a free parameter.

Thus in order for one to be confident at the 3σ level *a priori* that $w < w_0/2$, then depending on the dispersion regime for water vapor that applies (see Fig. 4), we require that $\sigma < 1.5\ mole/m^2$ (I, J, H bands),

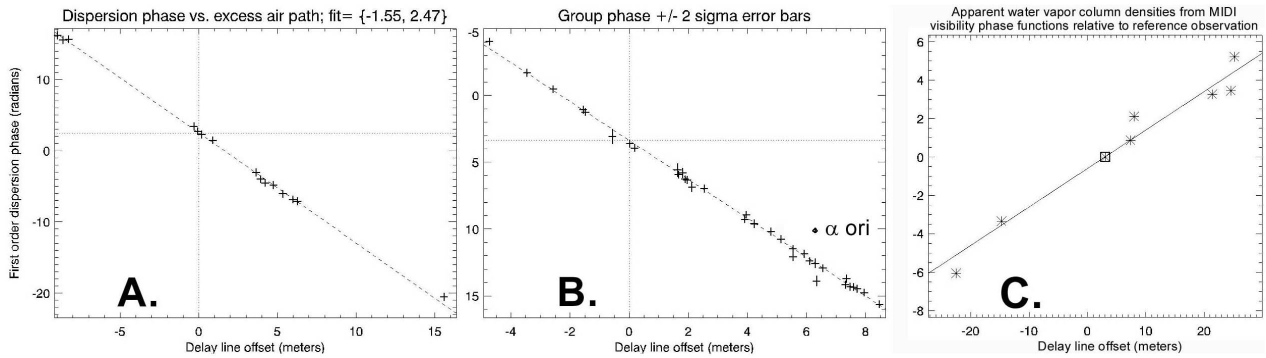

Figure 5. A: Group phase as a function of delay-line offset position, due to dispersion of delay-line air, for the 15 strongest observations on the night of 4 March 2003. Fitted slope is 1.545 $radians/meter$, slightly higher than expected (see text). **B:** Same as **A** but for all 37 observations performed on 12 October 2001. Fitted slope is 1.458 $radians/meter$, consistent with expectation. Error bars of $\pm 2\sigma$ are plotted. Additional scatter from the fit is believed to be due to very low frequency components of atmospheric water vapor fluctuations at a level of up to .30 radians rms. Observation of α ori past the first visibility null shows a group phase radically shifted from the fit, but also marginally inconsistent with the 180° offset expected for a symmetric star observed in the first visibility sidelobe (see text). **C:** Estimation of apparent differential water vapor columns using 8 calibrator observations by MIDI. In the N band (21 - 40 THz) the dominant source of delay-line air dispersion is due to its humid component (see Fig. 4, left graph).

$\sigma < .7\ mole/m^2$ (K band), $\sigma < .6\ mole/m^2$ (L, M bands), or $\sigma < .4\ mole/m^2$ (N band). In Sect. 4.1 we have met this criterion in the K band using VINCI. However the later results shown using MIDI have failed to reach this level of *a priori* dispersion calibration.

The results shown in Sect. 4.1 and 4.3 are based on fitting the slope and offset of first order dispersion versus delay-line position. In essence, we are using the interferometer to measure the humidity of the delay-line air! In the future, our intention is to directly measure the humidity of the delay-line air with sensors, and then calibrate the offset of the group phase with as little as one single calibrator observation. In that case, what performance do we require of the humidity monitoring system in order to meet the above criteria?

Again, in order to be able to unambiguously identify the correct branch of water vapor dispersion, the total uncertainty due to measurement error plus the incompletely averaged component of random atmospheric water vapor fluctuations, has to be guaranteed to be less than a half of a "bucket" of water vapor (or an rms of 1/6 of a bucket for confidence at the 3σ level). The requirement is most stringent in the N band where half of a bucket is 1.2 $mole/m^2$. The maximum possible delay-line offset for the VLTI is 120 meters. Thus in the worst case we need a measurement of the humidity in the VLTI with a guaranteed error of less than .01 $mole/m^3$ (equivalent to 1.4% *relative* humidity at 15°). The sensors which are being sent for tests (and eventual installation) at the VLTI appear to meet that requirement.[14] However this also assumes that the air inside the VLTI tunnels is homogenous, and that no unaveraged term from the atmosphere will remain. If there are indeed inhomogeneities in the indoor humidity, then multiple sensors with somewhat higher precision will be required to gauge the difference between the two complete light paths, again with a net error guaranteed to be less than 1.2 $mole/m^2$.

4. MEASUREMENT OF DELAY-LINE DISPERSION AT THE VLTI

In order to test our understanding of, and ability to calibrate, dispersion due to (humid) delay-line air at the VLTI, a number of tests were made using data from the VINCI and MIDI instruments.

4.1. First Order Dispersion of Delay-Line Air in K Band

A dispersive phase factor according to (8) may be observed directly using multiple observations of stars (ones expected to have zero visibility phase) over a range of differential delay-line position L. In the visible and near infrared, dry air is quite dispersive, and its dispersive effect is strongly seen as L changes by only a few meters. At

K band, a complete 2π wraparound in the group phase occurs for about every 4 meters of differential delay-line path.[15] This coefficient is somewhat dependent on the water vapor content of the air.

In Fig. 5A we plot the first order dispersion phase observed during a night of VINCI observations using a 24 meter VLTI baseline. Out of 57 successful observations during the night of 4 March 2003, the 15 strongest integrated dispersion phasors were selected. The calculated group phases are plotted against the delay line offset (note that the 15 points plotted refer to observations at relatively random times during the night and of a number of different stars). A fit to the first order component of dispersion resulting from (8) has a slope of 1.545 $radians/meter$, which is a little bit higher than expected given the low humidity during that night. The plot shown in Fig. 5B, for the night of 12 October 2001, is fit with a slope of 1.458 $radians/meter$. This could be explained, for instance, with air having a .3% water vapor content (corresponding to a relative humidity of 9% at the indoor temperature of 15° C), a little higher than the composition of the outside air at the time*.

The residuals about the fit shown in Fig. 5A had an rms level of .41 radians. All of the measurements had substantially lower formal error bars, which, if subtracted in quadrature, leave .38 radians rms unaccounted for. Some or all of this could be due to very low frequency components of atmospheric water vapor fluctuations. These observations each had a duration of about 3 minutes. Thus for that night we can place an upper limit on differential atmospheric water vapor column density fluctuations at frequencies lower than about .005 Hz of about $.38/K_{water}$ or .3 $mole/m^2$ rms. The example shown in Fig. 5B has a slightly lower, but similar residual of .34 radians rms (.30 radians after accounting for the contribution due to measurement noise).

4.2. Second Order Dispersion of Delay-Line Air in K Band

In addition to detecting first order dispersion due to the dispersion of delay-line air, we have obtained values for higher order dispersion based on results using quasi-coherent integration of VINCI data. Using rather long differential delay-line paths (of up to 100 meters), we expect and observe very substantial dispersive phase functions reflecting the second and higher order dispersion of moist delay-line air. Recall that the quasi-coherent integration method cancels the first order component of dispersive phase, but leaves all higher order terms intact.

Again, imagine that we are observing an unresolved star, or one that we can safely assume has a symmetric image and thus a visibility phase which is identically zero. Again, the excess delay-line air will contribute a dispersion which varies from observation to observation according to that differential path. After cancellation of the large (and usually wrapped around 2π) first order group phase, the higher order phase function is observed to reach an amplitude of about 1 radian peak-to-peak over the usable frequency range (127 - 151 THz) for 100 meters of delay-line air (about 3100 $mole/m^2$ at Paranal).

To quantify this effect, we gauged only the second order component (phase delay $\sim \nu^{-2}$). On the night of 11 April 2003, 45 VINCI observations of science and calibrator stars were performed, over a large range of delay-line positions. The amplitudes of the second order component of 12 randomly selected observations were measured and are plotted in Fig. 6A. An empirical fit to the data points is shown in a dashed line, and it can be seen that the amplitudes of these phase functions indeed are in proportion to the excess delay-line air paths. Plotted in bold is the relation that we would have expected due to the refractive index model of dry air. That slope would in fact be reduced due to water vapor present in the air (since water vapor has an opposite second order dispersion than dry air at this wavelength). However the empirical fit (dashed line) would require a water vapor content in the air of almost 1%, about 3 times higher than the humidity content of the outside air, which we do not believe could be the case. More likely there is a problem with our model for dry air.

Modelling the effect on the visibility phase due to a known column of delay-line air, is essential to proper phase calibration of an instrument using these paths. After removal of the second order components of phase whose amplitudes are plotted in Fig. 6A, the residual phases measured by VINCI ranged from .02 to .11 radians rms. The reduction in the phase residuals for one observation is shown in Fig. 6B-D, in which the measured second order phase shown in B has been cancelled with the addition of modelled air dispersion corresponding to 1780 $mole/m^2$ (rather than the actual 2840 $mole/m^2$). The residual phase which has thereby been reduced by an order of magnitude, is shown in C (and in D, expressed as phase delay). One can immediately see that the

*These calculations also assume (and are rather sensitive to) measurement of dispersion at an effective optical frequency of 137 THz which was not assured during the reductions.

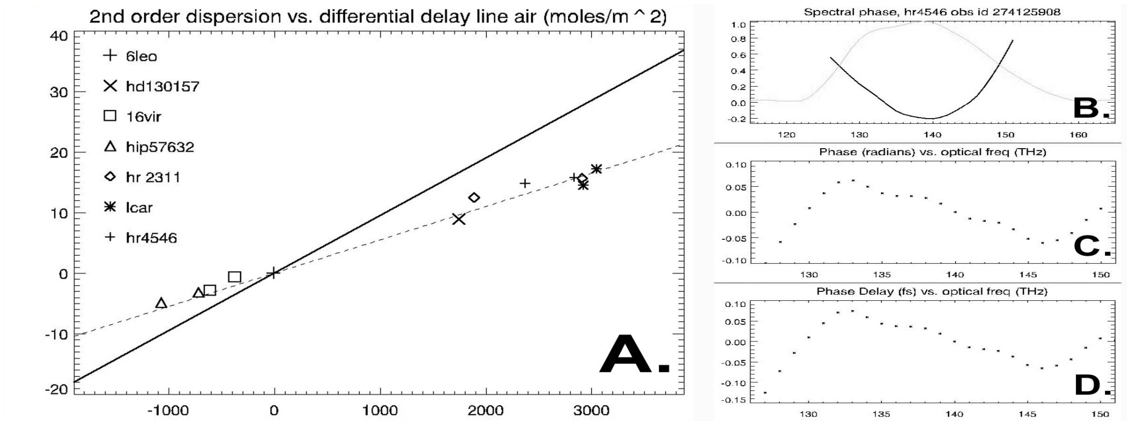

Figure 6. A: The second order component of dispersion is extracted from quasi-coherently integrated VINCI observations performed on 11 April 2003. These are plotted against excess delay-line air column densities in $mole/m^2$ (representing excess delay-line lengths of up to about 100m). Any phase function resulting from the stellar image (not expected for any of these objects) would appear as an offset from the fit. Thick line corresponds to the expected slope for dry air using our refractive index model, which is clearly contradicted by the data. **B:** The phase function (in radians vs. optical frequency) of one such observation. The amplitude spectrum of the coherently integrated flux is shown in grey, for reference. **C:** The phase function for the same observation *after* correction for 1780 $mole/m^2$ of dry air according to our current model. Note that this differs from the actual differential delay-line air column of 2840 $mole/m^2$. **D:** Same as **C**, expressed in phase delay. Note that the residual phase function has definite structure, not expected from the underlying source image, but possibly due to a refractive index modelling error.

residual phase has a definite structure, perhaps indicating a further deficiency in our understanding of delay-line air dispersion (we do not believe this represents a feature of the source).

4.3. Dispersion from Humid Delay-Line Air in N Band

Towards longer wavelengths, the predominant dispersive constituent of air is its water vapor component. The maximum expected water vapor content of the VLTI indoor air is about .4 $mole/m^3$. The maximum possible differential delay-line offset is 120 meters. Thus we could experience differential dispersion due to as much as 50 $mole/m^2$ of water vapor. A more typical value would be of order 10 $mole/m^2$. In the N band, this is the equivalent of 4 "buckets" of water vapor, that is, 4 complete rotations in the group phase. In addition to such a large first order dispersion, there is quite a significant amount of higher order dispersion also present. For instance, 10 $mole/m^2$ of water vapor dispersion causes a phase function over the N band of 54^o peak-to-peak amplitude.

MIDI is the N band interferometric instrument installed at the VLTI. A quasi-coherent reduction package[1] has been in routine use and in addition to delivering visibility amplitudes, supplies phase estimates over the N band with rms errors often better than 1^o. This level of phase accuracy is more than sufficient to unambiguously detect higher order dispersion due to water vapor present in the delay-line air, especially over long delay-line offsets, as has been reported on at this conference.[16]

Here we describe estimations of water vapor column densities using observations over relatively short delay-line offsets ($<$ 25m) employing *first-order* dispersion estimates obtained using coherent integration with tracking of water vapor dispersion. The result of one such reduction is shown in Fig. 7. The water vapor tracking estimate (top middle) has been adjusted to have an average value of zero over the duration of the observation, the remainder being assigned to the resulting phase function (bottom left). From that phase function, an estimate of dispersion due to remaining differential water vapor could be performed.

On the night of 1 February 2004, MIDI performed a number of technical observations on calibrator stars. Over a 4 hour period 15 successful results were obtained observing α tau and β lep. For each observation a fitting procedure was performed manually in order to estimate the excess water vapor column relative to an arbitrary

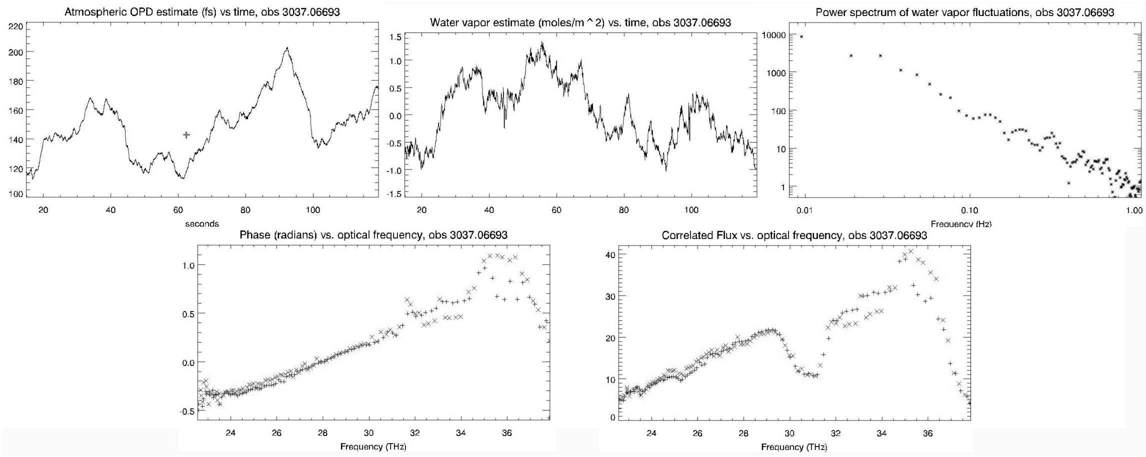

Figure 7. Results for one MIDI observation which has been processed using coherent integration with dispersion tracking. Algorithm simultaneously tracks achromatic OPD (upper left) and dispersive water vapor estimate (middle). Apparent power spectrum of atmospheric water vapor fluctuations also shown (top right). Coherent integration supplies estimate of phase function (combining effects of instrumental and possible source phase) and amplitude of correlation (bottom).

"reference" observation. Among the 15 observations, 8 supplied phase functions which had a sufficiently low noise level so that the correct branch (integer number of "buckets") of water vapor could be identifed with little ambiguity. In other words, spurious higher order water vapor dispersion was introduced and clearly visible for all but one branch. In Fig. 5C these estimated water vapor column densities are plotted (in $mole/m^2$) with respect to the unbalanced delay-line path in meters.

During the period of these observations, the water vapor content of the outdoor air varied between .54% and .70%. Based on that concentration, the expected indoor humidity would have been approximately .20 $mole/m^3$. A line of that slope, passing through the "reference" observation, is plotted in Fig. 5C (note that this is not a fit to the data; it is a plot of the *expected* slope with a rather arbitrary offset).

We can see that while the overall slope of the data is consistent with the presumed indoor humidity (there were no indoor humidity sensors at the VLTI), we notice a scatter around the plotted line which is rather large. It is quite a bit larger, in fact, than the scatter observed in the VINCI observation sets plotted in Fig. 5A and B from which we had inferred an underlying rms scatter of only .3 $mole/m^2$. The difference could *possibly* be explained by the longer baseline (47 meters compared to 16 meters for the VINCI data), and consequently a larger residual low-frequency component of atmospheric water vapor fluctuations. The VINCI and MIDI observations were of similar duration (a few minutes). Or it is possible that we are being affected by fluctuating indoor humidity inhomogeneities: the MIDI observations used the Unit Telescopes (UT's) instead of the siderostats, which are connected to the delay line tunnel through much longer light ducts.

Regardless of the source of the scatter seen in Fig. 5C, such a level of unpredictability is rather troubling if it cannot be reduced. In particular, one of the observations has an offset equal to about one half of a bucket (or 1.2 $mole/m^2$). That means that even if the indoor humidity had been known *a priori* (or equivalently, if a fit had been performed using other calibrator observations, as are plotted in Fig. 5C), then a measurement of the first order component of the phase function of such an observation would *not* suffice to constrain the branch of the water vapor dispersion phase function as we had required in Sect. 3.2.3. In order to reach that goal, apparently, further study is required to determine the source of these uncertainties. This might simply involve longer observations in order to better average the atmospheric random process, or more detailed monitoring or control of the humidity inside of the VLTI infrastructure. An upcoming experiment[14] may shed further light regarding the indoor environment which may lead to recommendations for a solution.

ACKNOWLEDGMENTS

We wish to acknowledge that some data included herein is based on observations made with the European Southern Observatory telescopes obtained from the ESO/ST-ECF Science Archive Facility and from the MIDI commissioning team.

REFERENCES

1. W. Jaffe, "Coherent Fringe Tracking and Visibility Estimation for MIDI," in *Proc. SPIE 5491, (these proceedings)*, 2004.
2. A. Quirrenbach, D. Mozurkewich, D. F. Buscher, C. A. Hummel, and J. T. Armstrong, "Phase-referenced visibility averaging in optical long-baseline interferometry," *Astronomy and Astrophysics* **286**, pp. 1019–1027, June 1994.
3. M. M. Colavita, "Fringe Visibility Estimators for the Palomar Testbed Interferometer," *Publications of the Astronomical Society of the Pacific* , pp. 111–117, 1999.
4. C. A. Hummel, D. Mozurkewich, J. A. Benson, and M. Wittkowski, "Coherent integration using phase bootstrapping," in *Interferometry for Optical Astronomy II. Edited by Wesley A. Traub . Proceedings of the SPIE, Volume 4838, pp. 1107-1114 (2003).*, pp. 1107–1114, Feb. 2003.
5. J. A. Meisner, "Scientific and technical results from VINCI using coherent estimation of fringe visibility," *Astrophysics and Space Science* **286**, pp. 119–127, 2003.
6. J. A. Meisner and R. S. Le Poole, "Dispersion affecting the VLTI and 10 micron interferometry using MIDI," in *Interferometry for Optical Astronomy II. Edited by Wesley A. Traub. Proceedings of the SPIE, Volume 4838, pp. 609-624 (2003).*, pp. 609–624, Feb. 2003.
7. R. J. Mathar, "Calculated refractivity of water vapor and moist air in the atmospheric window at 10μm," *Applied Optics* **43**, pp. 928–932, Feb. 2004.
8. M. M. Colavita, M. R. Swain, R. L. Akeson, C. D. Koresko, and R. J. Hill, "Effects of Atmospheric Water Vapor on Infrared Interferometry," *Publications of the Astronomical Society of the Pacific* **116**, Sept. 2004.
9. P. E. Ciddor, "Refractive index of air: new equations for the visible and near infrared," *Applied Optics* **35**, pp. 1566–1573, 1995.
10. J. Meisner, "Fringe tracking and group delay tracking methods for MIDI," in *From optical to millimetric interferometry: scientific and technological challenges. Proceedings of the 36th Liège International Astrophysics Colloquium, Liège, Belgium, July 2-5, 2001. Edited by J. Surdej, J. P. Swings, D. Caro, and A. Detal. Liège, Belgium: Université de Liège, Institut d'Astrophysique et de Géophysique, 2001, p. 225 - 231*, pp. 225–231, 2001.
11. C. D. Koresko, B. P. Mennesson, E. Serabyn, M. Colavita, R. L. Akeson, and M. R. Swain, "Longitudinal dispersion control for the Keck interferometer nuller," in *Interferometry for Optical Astronomy II. Edited by Wesley A. Traub. Proceedings of the SPIE, Volume 4838, pp. 625-635 (2003).*, pp. 625–635, Feb. 2003.
12. M. M. Colavita, "Phase referencing for stellar interferometry," in *High-Resolution Imaging by Interferometry II, ESO Conference and Workshop Proceedings No. 39, Edited by J. M. Beckers and F. Merkle*, pp. 845–851, Mar. 1992.
13. O. P. Lay, "The temporal power spectrum of atmospheric fluctuations due to water vapor," *Astronomy and Astrophysics Supplement Series* **122**, pp. 535–545, May 1997.
14. S. Albrecht, E. J. Bakker, J. A. de Jong, R. N. Tubbs, J. A. Meisner, and R. S. le Poole, "Calibration of temperature and relative humidity sensors for use on the VLT-Interferometer," in *Proc. SPIE 5491, (these proceedings)*, 2004.
15. R. L. Akeson, M. R. Swain, and M. M. Colavita, "Differential phase technique with the Keck Interferometer," in *Proc. SPIE 4006, Interferometry in Optical Astronomy, Pierre J. Lena; Andreas Quirrenbach; Eds.*, pp. 321–327, July 2000.
16. R. N. Tubbs, J. A. Meisner, E. J. Bakker, and S. Albrecht, "Differential phase delay observations with VLTI/MIDI at N-band," in *Proc. SPIE 5491, (these proceedings)*, 2004.